Inverse problem for light emission from weakly deformed microdisk cavities

Marcus Kraft and Jan Wiersig
Institut für Theoretische Physik, Otto-von-Guericke-Universität Magdeburg, Postfach 4120, D-39016 Magdeburg, Germany
(Received 1 June 2016; published 28 July 2016)

Microdisk cavities with a smoothly deformed boundary allow for highly directional light emission. The conventional direct problem is to determine the far-field emission pattern of an optical mode for a given cavity shape by solving Maxwell's equations. We introduce the inverse problem of finding the cavity shape for which the far-field intensity pattern of the optical mode best fits a desired profile. We find an optimal solution within a second-order perturbation theory for weakly deformed cavities with a mirror reflection symmetry. Surprisingly, in this case the optimal solution is unique for specified mode numbers and refractive index. The perturbative results are confirmed by full numerical simulations.

DOI: 10.1103/PhysRevA.94.013851

I. INTRODUCTION

Optical microcavities have played a significant role in fundamental and applied research in the past decade [1]. A popular geometry is the microdisk [2–4], which confines light by total internal reflection at the circular-shaped dielectric boundary. The optical modes in such a cavity are called whispering-gallery modes. These modes have high-quality factors $Q = \omega\tau$, where τ is the lifetime and ω is the resonance frequency of the given mode. The in-plane light emission from an ideal microdisk is isotropic due to the rotational symmetry, which is a considerable disadvantage for applications. To overcome this problem, microcavities with deformed boundaries have been suggested and fabricated [5–9]. For various shape deformations, unidirectional emission, i.e., emission into a single direction with small angular spread, has been demonstrated [10–23]. A recent review provides an in-depth account of the rich physics of deformed microcavities [24].

When the boundary deformation is weak in the sense that the perturbation area is small compared to the wavelength squared, it is possible to compute the Q-factor, the frequency ω, the spatial mode pattern, and the far-field pattern using a perturbation theory [25,26]. This second-order perturbation theory is nontrivial, as an optical microcavity is an open system. Several shapes have been considered: the cut disk cavity [25], cavities subjected to local boundary perturbations [27], and the limaçon cavity [28]. The perturbation theory has given great insight into an extreme sensitivity of the far-field pattern observed in cavities with subwavelength boundary deformations [26]. Moreover, it allows a description of multimode coupling in terms of boundary-wave scattering [29].

The perturbation theory, and in fact all theory, numerical simulations, and experiments done so far on deformed microdisk cavities, treat the direct problem; see the illustration in Fig. 1. It consists of determining the far-field emission pattern of an optical mode for a given boundary shape. In this paper, we introduce the corresponding inverse problem of finding the cavity shape for which the far-field intensity pattern of an optical mode best matches the desired pattern. We show that within the second-order perturbation theory, an optimal solution of the inverse problem exists and is unique. The inverse problem is not only interesting from the academic point of view, but it can also serve as a useful tool to design

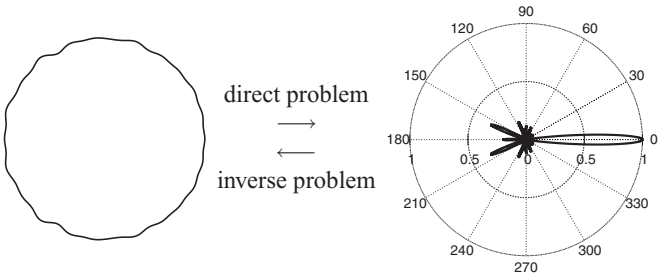

FIG. 1. Deformed boundary of a microdisk cavity (left) and in-plane far-field intensity pattern of a corresponding optical mode in a polar plot (right). The direct problem consists in solving Maxwell's equations to determine the far-field pattern of an optical mode for a given cavity shape. In the opposite case of the inverse problem, the far-field intensity pattern of the optical mode is known, and the best-fitting cavity shape is to be determined.

microcavity devices suitable for various kinds of applications. Moreover, there are situations in which the shape of a cavity is difficult to measure experimentally, but the far-field intensity pattern can be accurately determined; see [30]. In this case, the inverse problem may allow us to extract the cavity shape from the observed far-field data.

Inverse problems enjoy a long history in science and engineering, and several textbooks on this topic are available, e.g., [31]. We briefly remark on inverse problems related to the one discussed in this paper. The most similar one appears to be the pump-controlled light emission from random lasers [32]. The fixed geometry consists of small dielectric scatterers randomly placed within a two-dimensional circular area. In the weak-scattering regime, the direct problem is to determine the far-field pattern for a given spatially nonuniform pumping profile. The inverse problem, i.e., finding the nonuniform pumping profile leading to a desired far-field pattern, has been treated by brute-force numerics. Note that nonuniform pumping has also been used for microdisk lasers to control the emission directionality [33] but not on the basis of an inverse problem.

Another similar problem is the inverse problem of antenna theory, namely the determination of a line source current distribution from its radiation pattern; see [34]. In our case, however, there is no current distribution; the far-field pattern is directly associated with a given electromagnetic mode of

the cavity. Another class of inverse problems is the inverse scattering problem; for a review of such problems, e.g. in acoustics, see Ref. [35]. The inverse-scattering problem is to determine the shape of an obstacle (usually Dirichlet or Neumann boundary conditions) from the knowledge of the time-harmonic incident wave and the far-field pattern of the scattered wave. In our case, there is no incident wave; the outgoing wave is emitted from inside the cavity according to the electromagnetic boundary conditions. There is also a loose relation to the famous question, "Can one hear the shape of a drum?" by Kac [36]. The inverse problem is to find the shape of a drumhead for a given (infinite) set of acoustic eigenfrequencies. In contrast to our problem, Kac's inverse problem does not generally possess a unique solution giving a negative answer to the above question [37].

The outline of the paper is as follows. In Sec. II we recapitulate the perturbation theory for deformed microdisks. To present the perturbative expressions in a more convenient form, Sec. III provides a reformulation in terms of a Fourier basis. Section IV A is devoted to our theory of solving the inverse problem. Numerical results are presented in Sec. IV B. Section V contains a summary.

II. PERTURBATION THEORY

In this section, we briefly recapitulate the perturbation theory for passive cavity modes in weakly deformed microdisks introduced by Dubertrand *et al.* [25]. As in most studies of microdisk cavities, the mode properties are computed in a two-dimensional configuration within the effective index approximation. Inside the cavity, the effective refractive index is $n > 1$. Outside the cavity, the refractive index is assumed to be unity. The perturbed boundary is given in polar coordinates

$$\frac{r(\theta)}{R} = 1 + \varepsilon f(\theta), \tag{1}$$

with single-valued, 2π-periodic, and dimensionless deformation function $f(\theta)$ and formal perturbation parameter ε. For $\varepsilon \to 0$, the boundary converges to a circle of radius R. The theory in Ref. [25] is restricted to TM polarization (for TE polarization, see [26]) and to boundary deformations with mirror-reflection symmetry, i.e., $f(-\theta) = f(\theta)$. Most cavities studied in the literature have such a symmetry, e.g., [6,7,15], although some counterexamples do exist; see [10,38,39]. In the situation with mirror-reflection symmetry, the modes can be divided into two symmetry classes, one with positive and one with negative parity with respect to the symmetry line. The formulas given below are restricted to modes with positive parity.

The basic idea is to expand the solutions of the perturbed cavity in terms of the well-known solutions of the unperturbed circular cavity. A mode with fixed parity in a circular cavity is characterized by an azimuthal mode number $m \geqslant 0$ and a radial mode number $l > 0$. The frequency of the mode can be written as a dimensionless quantity, $x_0 = \omega_0 R/c = k_0 R$; c is the vacuum speed of light and k_0 is the wave number. The frequency is a complex number due to the outgoing-wave conditions. The real part is the usual frequency and the imaginary part determines the decay rate of the mode. Inside and outside of the deformed cavity, the expansion for fixed mode numbers m and l is given by

$$\Psi_1(r,\theta) = \frac{J_m(nkr)}{J_m(nx)}\cos(m\theta) + \sum_{p\neq m} a_p \frac{J_p(nkr)}{J_p(nx)}\cos(p\theta), \tag{2}$$

$$\Psi_2(r,\theta) = (1+b_m)\frac{H_m^{(1)}(kr)}{H_m^{(1)}(x)}\cos(m\theta) + \sum_{p\neq m}(a_p+b_p)\frac{H_p^{(1)}(kr)}{H_p^{(1)}(x)}\cos(p\theta), \tag{3}$$

with expansion coefficients $a_p, b_p \in \mathbb{C}$, the Bessel function J_m of order m, and the Hankel function $H_m^{(1)}$ of the first kind and order m. The sums run over all non-negative p excluding $p = m$. Up to second order in ε, the perturbed frequency $x = kR \in \mathbb{C}$ and the expansion coefficients turn out to be

$$x = x_0\left[1 - \varepsilon A_{mm} + \varepsilon^2\left(\frac{3A_{mm}^2 - B_{mm}}{2} + x_0\left(A_{mm}^2 - B_{mm}\right)\frac{H_m^{(1)\prime}}{H_m^{(1)}}(x_0) - (n^2-1)x_0\sum_{k\neq m}\frac{A_{mk}A_{km}}{S_k(x_0)}\right)\right] + O(\varepsilon^3), \tag{4}$$

$$a_p = \varepsilon x_0(n^2-1)\frac{1}{S_p(x_0)}\left(A_{pm} + \varepsilon\left\{A_{pm}A_{mm}\left(\frac{x_0}{S_p(x_0)}\frac{\partial S_p}{\partial x}(x_0) - 1\right) + \frac{1}{2}B_{pm}\left[1 + x_0\left(\frac{H_m^{(1)\prime}}{H_m^{(1)}}(x_0) + \frac{H_p^{(1)\prime}}{H_p^{(1)}}(x_0)\right)\right] + x_0(n^2-1)\sum_{k\neq m}\frac{A_{pk}A_{km}}{S_k(x_0)}\right\}\right) + O(\varepsilon^3), \tag{5}$$

$$b_p = \varepsilon^2\frac{1}{2}x_0^2(n^2-1)B_{pm} + O(\varepsilon^3). \tag{6}$$

Here, the following definition is used:

$$S_p(x) := n\frac{J_p'}{J_p}(nx) - \frac{H_p^{(1)\prime}}{H_p^{(1)}}(x) \tag{7}$$

and the coupling matrices

$$A_{pm} = \frac{\varepsilon_p}{\pi}\int_0^\pi f(\theta)\cos(p\theta)\cos(m\theta)\,d\theta, \tag{8}$$

$$B_{pm} = \frac{\varepsilon_p}{\pi}\int_0^\pi f^2(\theta)\cos(p\theta)\cos(m\theta)\,d\theta, \tag{9}$$

with

$$\varepsilon_p := \begin{cases} 2 & \text{for } p \neq 0, \\ 1 & \text{for } p = 0, \\ 0 & \text{for } p < 0. \end{cases} \tag{10}$$

All the relevant information of the deformation function $f(\theta)$ is encoded in the coupling matrices A_{pm} and B_{pm}, which determine the contribution of the circular cavity modes to the considered mode of the perturbed cavity.

The far-field amplitude $F(\theta)$ follows from Eq. (3) and the asymptotic behavior of the Hankel function for large r,

$$\Psi_2(r,\theta) = \sqrt{\frac{2}{\pi kr}} e^{i(kr-\pi/4)} F(\theta), \tag{11}$$

$$F(\theta) = (1+b_m)\frac{e^{-i\pi\frac{m}{2}}}{H_m^{(1)}(x)}\cos(m\theta) + \sum_{p\neq m}(a_p+b_p)\frac{e^{-i\pi\frac{p}{2}}}{H_p^{(1)}(x)}\cos(p\theta). \tag{12}$$

The theory is formally valid in the perturbative regime,

$$s_n \frac{\delta a}{8\pi} k^2 n^2 \ll 1, \tag{13}$$

with

$$s_n = 1 - \frac{2}{\pi}\left(\arcsin\frac{1}{n} + \frac{1}{n}\sqrt{1-\frac{1}{n^2}}\right) \tag{14}$$

and δa being the area where the perturbation in terms of the refractive index is nonzero. However, numerical simulations indicate that the second-order perturbation theory gives reliable results also for much larger δa [28].

III. FOURIER EXPANSION

For the purpose of this paper, it is convenient to express the relevant functions appearing in the perturbation theory from Sec. II in terms of Fourier expansions. The deformation function and its square can be written as

$$\varepsilon f(\theta) = \frac{\tilde{a}_0}{2} + \sum_{j=1}^{\infty}\tilde{a}_j\cos(j\theta), \tag{15}$$

$$\tilde{a}_j = \frac{2}{\pi}\int_0^{\pi}\varepsilon f(\theta)\cos(j\theta)\,d\theta, \tag{16}$$

$$\varepsilon^2 f^2(\theta) = g(\theta) = \frac{\tilde{b}_0}{2} + \sum_{j=1}^{\infty}\tilde{b}_j\cos(j\theta), \tag{17}$$

$$\tilde{b}_j = \frac{2}{\pi}\int_0^{\pi} g(\theta)\cos(j\theta)\,d\theta. \tag{18}$$

A straightforward calculation relates the Fourier coefficients $\tilde{a}_j$ and $\tilde{b}_j$,

$$\tilde{b}_j = \begin{cases} \frac{1}{2}\tilde{a}_0^2 + \sum_{n=1}^{\infty}\tilde{a}_n^2 & \text{for } j=0, \\ \tilde{a}_0\tilde{a}_j\kappa_j + \frac{1}{2}\sum_{n=1}^{\infty}\tilde{a}_n(\tilde{a}_{j-n}\kappa_{j-n} & \\ \quad +\tilde{a}_{j+n}\kappa_{j+n} + \tilde{a}_{n-j}\kappa_{n-j}) & \text{for } j>0, \end{cases} \tag{19}$$

with

$$\kappa_j := \begin{cases} 0 & \text{for } j \leqslant 0, \\ 1 & \text{for } j \geqslant 1. \end{cases} \tag{20}$$

The Fourier coefficients $\tilde{a}_j$ and $\tilde{b}_j$ are used to write the coupling matrices as

$$A_{pm} = \frac{\varepsilon_p}{4}[\tilde{a}_0(\delta_{p,m}+\delta_{p,-m}) + \tilde{a}_{p-m}\kappa_{p-m} + \tilde{a}_{m+p}\kappa_{m+p} + \tilde{a}_{m-p}\kappa_{m-p}], \tag{21}$$

$$B_{pm} = \frac{\varepsilon_p}{4}[\tilde{b}_0(\delta_{p,m}+\delta_{p,-m}) + \tilde{b}_{p-m}\kappa_{p-m} + \tilde{b}_{m+p}\kappa_{m+p} + \tilde{b}_{m-p}\kappa_{m-p}] \tag{22}$$

with the Kronecker delta $\delta_{i,j}$.

In the same spirit, we rewrite the far-field amplitude $F(\theta)$ in Eq. (12) as

$$F(\theta) = h_m\cos(m\theta) + \sum_{\substack{p=0 \\ p\neq m}}^{\infty} h_p\cos(p\theta) \tag{23}$$

with

$$h_m = (1+b_m)\tilde{H}_m, \tag{24}$$

$$h_p = (a_p+b_p)\tilde{H}_p \quad \text{for } p\neq m, \tag{25}$$

$$\tilde{H}_j := \frac{\kappa_{j+1}e^{-i\pi\frac{j}{2}}}{H_j^{(1)}(x)}. \tag{26}$$

Equally, we expand the far-field intensity $I(\theta) = |F(\theta)|^2$,

$$I(\theta) = \sum_{p=0}^{\infty}\frac{\varepsilon_p}{2}f_p\cos(p\theta), \tag{27}$$

$$f_p = \frac{2}{\pi}\int_0^{\pi} I(\theta)\cos(p\theta)\,d\theta, \tag{28}$$

with

$$f_p = \frac{1}{2}\sum_{k=0}^{\infty}h_k(h_{k-p}^* + h_{p-k}^* + h_{k+p}^* + h_0^*\delta_{p,0}\delta_{k,0}). \tag{29}$$

IV. INVERSE PROBLEM

A. Theory

Next we study the inverse problem within the second-order perturbation theory from Sec. II using the Fourier expansion from Sec. III. We restrict ourselves to modes with positive parity. The extension to negative parity is straightforward.

The perturbation theory naturally solves the direct problem $f(\theta) \to I(\theta)$, i.e., the far-field intensity pattern $I(\theta)$ is computed from the deformation function $f(\theta)$. The parameter set (m,l,n) consists of the mode numbers m, l and the refractive index n. The inverse problem $G(\theta) \to f(\theta)$ starts with a given far-field intensity pattern $G(\theta) \geqslant 0$ and ends with the boundary shape. The given far-field intensity pattern is normalized to unity by $\int_0^{2\pi} G(\theta)\,d\theta = 1$. We formulate this problem as the least-square optimization of an appropriate cost functional,

which measures the difference between the desired profile $G(\theta)$ and the resulting far-field intensity pattern $I(\theta)$,

$$L(\{\tilde{a}_i\},m,l) = \int_0^{2\pi} [\alpha G(\theta) - I(\{\tilde{a}_i\},m,l,\theta)]^2 d\theta \tag{30}$$

with the Fourier coefficients $\tilde{a}_j$ of the deformation function $f(\theta)$. The real-valued normalization factor α depends on the yet unknown boundary deformation via

$$\alpha = \int_0^{2\pi} I(\{\tilde{a}_i\},m,l,\theta) d\theta. \tag{31}$$

We therefore treat the inverse problem as a bilevel optimization. The lower-level optimization task is to minimize L analytically while keeping α constant. This task is nested within the upper-level optimization task in which L is minimized numerically by varying α. As a good initial value for α, we identify the lowest-order result from the perturbation theory, $\alpha_0 = \pi |h_m^{(0)}|^2$.

Using the Fourier expansions (27) and

$$\begin{aligned} G(\theta) &= \sum_{j=0}^{\infty} \frac{\varepsilon_j}{2} g_j \cos(j\theta), \\ g_j &= \frac{2}{\pi} \int_0^{\pi} G(\theta) \cos(j\theta)\, d\theta, \end{aligned} \tag{32}$$

a tedious but straightforward calculation gives

$$\begin{aligned} L = {} & \alpha^2 \frac{\pi}{2} \sum_{j=0}^{\infty} \varepsilon_j g_j^2 - \alpha \frac{\pi}{2} \sum_{i,j=0}^{\infty} \varepsilon_j g_j h_i^* \\ & \times (h_{i-j} + h_{j-i} + h_{i+j} + h_0 \delta_{i,0} \delta_{j,0}) + \frac{\pi}{4} \sum_{i,j,k=0}^{\infty} h_i^* h_k^* h_j \\ & \times (h_{i+j-k} + h_{k+i+j} + h_{k+i-j} + h_{i-j-k} + h_{j+k-i} \\ & + h_{j-k-i} + h_{k-i-j} + h_0 \delta_{i,0} \delta_{j,0} \delta_{k,0}). \end{aligned} \tag{33}$$

The dependence on $\{\tilde{a}_i\},m,l$ is hidden in the Fourier coefficients. As we restrict ourselves to a second-order perturbation theory, we expand also the cost functional to second order,

$$L = L_0 + \sum_{i=0}^{\infty} d_i \tilde{a}_i + \frac{1}{2} \sum_{i,j=0}^{\infty} C_{ij} \tilde{a}_i \tilde{a}_j + O(\tilde{a}_i^3) \tag{34}$$

with

$$d_i = \left. \frac{\partial L}{\partial \tilde{a}_i} \right|_{\{\tilde{a}_j\}=0}, \quad C_{ij} = \left. \frac{\partial^2 L}{\partial \tilde{a}_i \partial \tilde{a}_j} \right|_{\{\tilde{a}_j\}=0}. \tag{35}$$

To compute d_i and C_{ij}, one first has to replace h_j in the cost functional (33) by the coefficients a_j and b_j using Eqs. (24)–(26). Here, one has to bear in mind that $\tilde{H}_j$ depends on the resonant frequency x. Second, a_j, b_j, and x have to be replaced by $\tilde{a}_j$ using Eqs. (4)–(6), Eqs. (21) and (22), and Eq. (19). Finally, the resulting expression for L has to be expanded in $\tilde{a}_j$ up to second order. We have done this calculation using the computer algebra system MATHEMATICA. The explicit result is far too long to be shown here.

Minimizing L leads to a linear set of equations,

$$\begin{pmatrix} C_{11} & \cdots & C_{1N} \\ \vdots & & \vdots \\ C_{N1} & \cdots & C_{NN} \end{pmatrix} \begin{pmatrix} \tilde{a}_1 \\ \vdots \\ \tilde{a}_N \end{pmatrix} = - \begin{pmatrix} d_1 \\ \vdots \\ d_N \end{pmatrix}, \tag{36}$$

where both Fourier spaces are consistently truncated at N leading to an even-determined problem. This linear problem can be uniquely solved for the Fourier coefficients $\tilde{a}_j$ of the deformation function provided that the square matrix C has full rank. Indeed, we find numerically for a variety of parameter sets and given far-field intensity patterns that this seems to be always the case.

Up to now we have treated the inverse problem for a fixed mode. Now, we discuss the possibility to optimize the boundary shape for several modes simultaneously. The simple strategy is to add the cost functionals for different m (different l are implicitly included) with weighting factors $w_m \geqslant 0$:

$$\mathcal{L}(\{\tilde{a}_j\}) = \sum_m w_m L(\{\tilde{a}_j\},m). \tag{37}$$

Again we end up with Eq. (36), where C_{ij} and d_i have to be replaced by

$$\hat{C}_{ij} = \sum_m w_m C_{ij}(m), \tag{38}$$

$$\hat{d}_i = \sum_m w_m d_i(m). \tag{39}$$

B. Numerical results

This section provides numerical results based on the theory developed in the previous sections. As examples for the target function $G(\theta) = G(-\theta)$, we choose directed emission into one, two, and six directions. We would like to mention that, with conventional personal computer technology, finding the optimal solution to the inverse problem takes typically just a few minutes.

The most interesting case for applications is directional emission into a single direction with a small angular spread. To study such a situation, we first consider as a given far-field intensity pattern $G(\theta)$ a normalized Gaussian function with standard deviation ($\approx$0.4247 full width at half-maximum) $\sigma = 0.04$ in radians (a Lorentz function gives similar results) placed at $\theta = 0$, corresponding to a very narrow emission profile. Strictly speaking, one should use an infinite sum of Gaussian functions placed at $\theta = 0, 2\pi, \ldots$, but in practice this is not needed, as for the chosen $\sigma \ll \pi$ the Gaussian function decays very rapidly such that the 2π-periodicity of $G(\theta)$ is not spoiled. Figure 2 shows the solution of the inverse problem for mode numbers $(m,l) = (16,1)$ and refractive index $n = 2$. The resulting cavity shape is depicted in Fig. 2(b). Its far-field emission profile $I(\theta)$ is plotted in the same panel as a polar plot and also in Fig. 2(a) in direct comparison to the desired pattern $G(\theta)$. A reasonable but not fully satisfactory agreement can be seen. To assess the performance of the perturbation theory itself, the far-field intensity $I(\theta)$ is compared to the result of full numerical calculations using the boundary element method (BEM) [40] based on the same boundary shape. No differences can be observed by eye. It is mentioned that the internal spatial

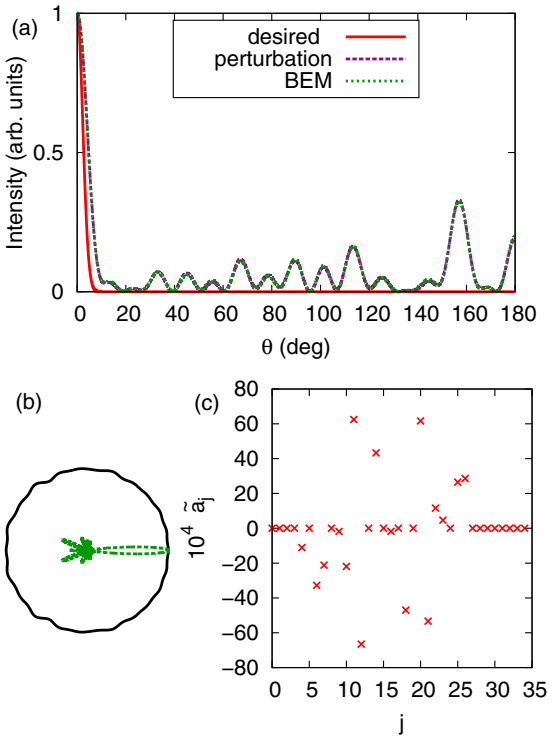

FIG. 2. Solution of the inverse problem for mode numbers $(m,l) = (16,1)$ and refractive index $n = 2$. The desired far-field intensity pattern is a Gaussian function with standard deviation $\sigma = 0.04$ in radians. (a) Desired far-field intensity pattern (solid red curve) and resulting far-field intensity pattern (dashed purple curve). The dotted green curve is computed by the BEM based on the same boundary shape. Both curves lie on top of each other. Note that only the interval $\theta \in [0,\pi]$ ($[0°,180°]$) is shown. The remaining part is given by symmetry. (b) Resulting boundary shape (solid curve) and corresponding far-field intensity pattern in a polar plot (green dashed). (c) Fourier coefficients $\tilde{a}_j$ (dimensionless) of the deformation function with $j = 1,\ldots,N$.

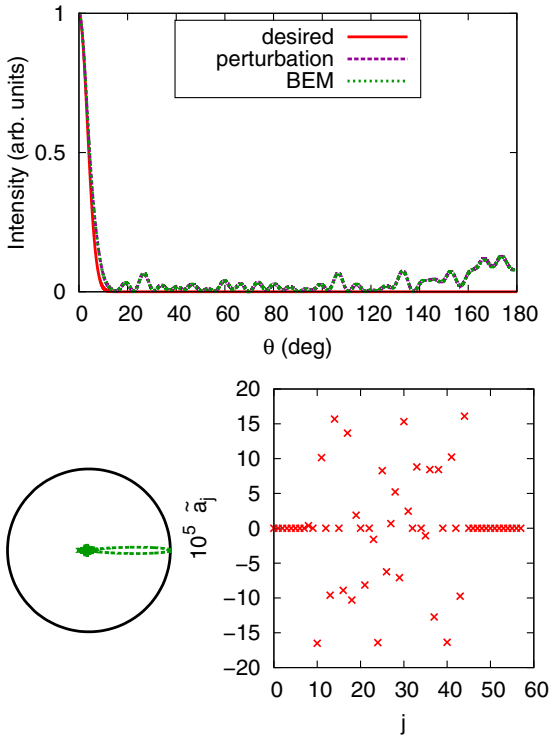

FIG. 3. Solution of the inverse problem for mode numbers $(m,l) = (27,1)$ and refractive index $n = 2$. The desired far-field intensity pattern is a Gaussian function with standard deviation $\sigma = 0.06$ in radians; cf. Fig. 2.

mode pattern is barely changed under the deformation (not shown).

Figure 2(c) shows the Fourier coefficients $\tilde{a}_j$ with $j = 1,\ldots,N$ of the deformation function $f(\theta)$. It can be seen that a broad range of coefficients contribute. The absolute values of the individual coefficients are, however, below 0.01.

Figure 3 contains an example with larger azimuthal mode number m. As a general trend, we observe that for larger m the inverse problem can be solved more accurately. A hand-waving argument is that a smaller wavelength along the azimuthal direction allows us to resolve small features of the given far-field pattern more easily. Moreover, we notice that for larger m, the size of the Fourier coefficients $\tilde{a}_j$ becomes smaller. Here, $|\tilde{a}_j| < 2\times10^{-4}$. The resulting cavity shape, therefore, looks very much like a circle. The tiny deformation is revealed by the deformation function $f(\theta)$ in Fig. 4. The observed bound $|f(\theta)| < 2\times10^{-3}$ corresponds to a variation of less than 20 nm for a 10-μm-radius cavity. Even though this is a very small variation, it is still one order of magnitude larger than the surface roughness of the high-Q silicon microdisk fabricated in Ref. [41]. Hence, it is possible to fabricate such slightly deformed cavities with present technology. It is interesting that such a tiny deformation can lead to a highly directional emission pattern. This extreme sensitivity of the far-field pattern to tiny deformations of the circular shape has been witnessed before [42–44]. It is worth mentioning that reducing N (the number of Fourier coefficients $\tilde{a}_j$) from 60 down to about 20 here still gives reasonably accurate solutions of the inverse problem.

The beam divergence in Fig. 3 of ±0.06 ($\pm3.4°$) is comparable to what has been achieved for the notched ellipse [21] and the shortegg cavity [23]. The former works best for the high refractive index regime $n \geqslant 3$ [45] and the latter exclusively in the low-index regime $1.5 \leqslant n \leqslant 1.8$. In our approach, the refractive index can be arbitrarily chosen. It is worth mentioning that the nice Gaussian profile that our approach delivers is advantageous for light coupling into a fiber.

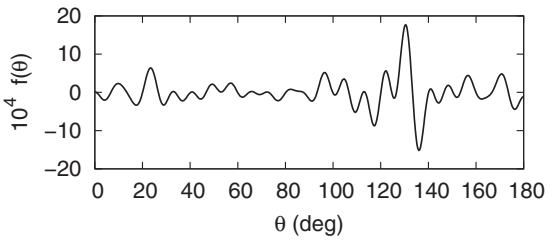

FIG. 4. Deformation function $f(\theta)$ (dimensionless) of the optimal solution from Fig. 3.

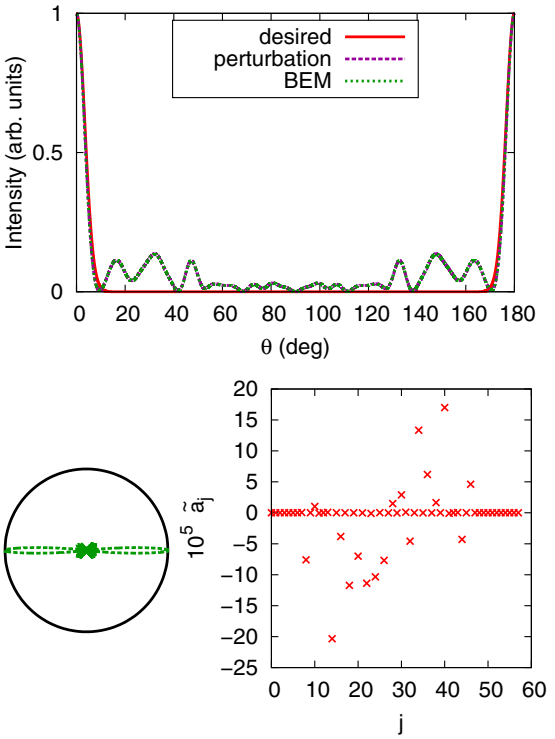

FIG. 5. Solution of the inverse problem with a desired far-field intensity pattern consisting of two Gaussian functions each with $\sigma = 0.06$. The parameter set is $m = 27$, $l = 1$, and $n = 2$; cf. Fig. 2.

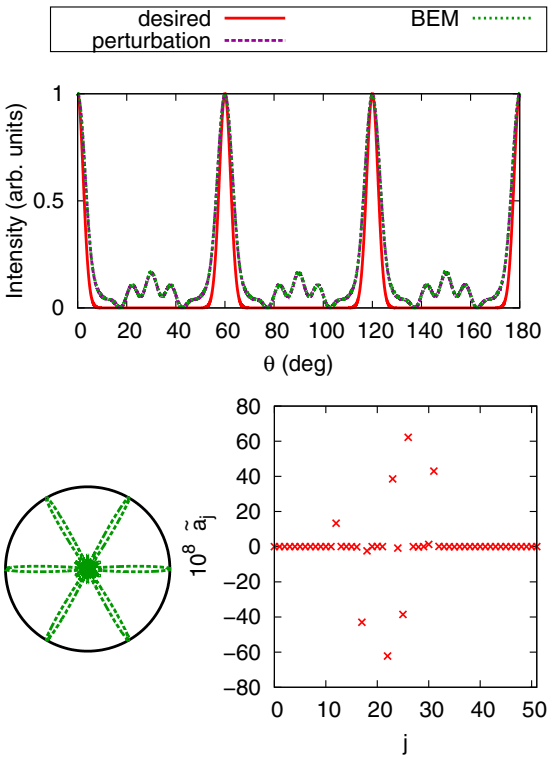

FIG. 6. Solution of the inverse problem with a desired far-field intensity pattern consisting of six equally spaced Gaussian functions with $\sigma = 0.04$. The parameter set is $m = 24$, $l = 1$, and $n = 3$; cf. Fig. 2.

Next, we make the desired far-field intensity pattern more complicated. Figure 5 shows the case in which the far-field intensity pattern consists of two Gaussian functions of equal standard deviation. The first Gaussian function is localized at $\theta = 0$ and the second one at $\theta = \pi$. The mode numbers are chosen to be $(m,l) = (27,1)$. Again, we find a very weak deformation ($|\tilde{a}_j| < 2.5\times10^{-4}$) that reproduces the desired far-field intensity pattern with high accuracy.

Figure 6 displays the case of a desired far-field intensity pattern consisting of six equally spaced Gaussian functions of equal standard deviation. Here, we choose $(m,l) = (24,1)$ and a larger refractive index, $n = 3$. The resulting boundary shape has an even weaker deformation ($|\tilde{a}_j| < 8 \times 10^{-7}$). It reproduces the desired far-field intensity pattern with high accuracy.

Figure 7 demonstrates that an optimal solution can also be found for several modes simultaneously. The equally weighted modes with azimuthal mode numbers $m = 20, 21$, and 22 have been used. Again, the deformation is weak ($|\tilde{a}_j| < 6\times10^{-4}$) and the desired profile is well reproduced.

Our results indicate that the far-field pattern can depend strongly on a tiny deformation of the circular boundary. Nevertheless, the far-field pattern itself is stable against further changes of the boundary shape. Changes of the Fourier coefficients of the boundary function below 5% only barely change the far-field pattern (not shown). This finding makes the emission robust with respect to a surface roughness well below the resulting boundary variations.

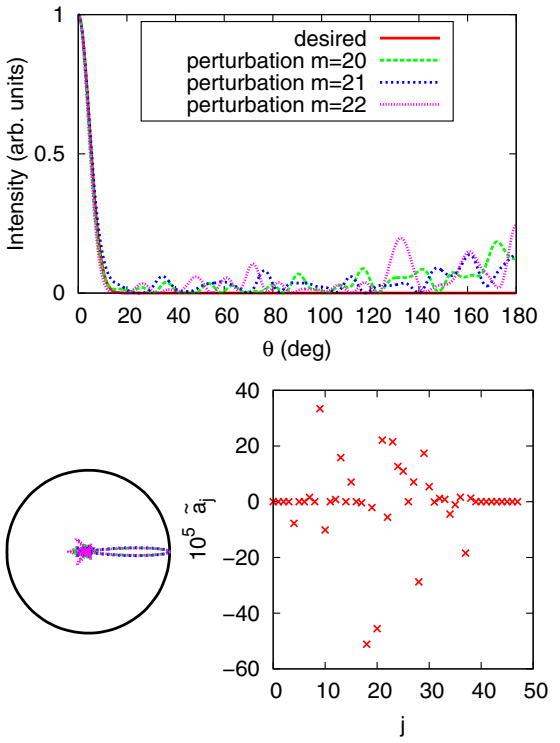

FIG. 7. Simultaneous solution of the inverse problem with a desired far-field intensity pattern consisting of a Gaussian function with $\sigma = 0.08$ for the modes with $m = 20$, 21, and 22. The other parameters are $l = 1$ and $n = 2$; cf. Fig. 2.

V. SUMMARY

We have introduced an inverse problem for weakly deformed microdisk cavities with mirror-reflection symmetry. Based on the far-field intensity data, the best-fitting shape of the microcavity can be determined. Within a second-order perturbation theory, the optimal solution of the inverse problem is unique for specified mode numbers and refractive index. In the regime where the perturbation theory is valid [Eq. (13)], we observed that with an increasing azimuthal mode number, the quality of the solution improves and the resulting deformation becomes weaker. Interestingly, even very weakly deformed cavities are capable of emitting in a highly directional manner. Comparison with full numerical solutions of Maxwell's equations have confirmed the perturbative results nicely.

This solution of the inverse problem might be useful for (i) the design of optical microcavity devices with a certain needed far-field pattern, (ii) determination of unknown cavity shapes from given far-field data, and (iii) achieving unidirectional light emission from very weakly deformed microdisk cavities (preserving an ultrahigh-quality factor) for any given refractive index. In the latter case, the experimental realization may require a very low surface roughness.

A generic far-field intensity pattern is only possible for a microcavity without mirror-reflection symmetry. To apply our theory of the inverse problem to this general case, first the perturbation theory of Dubertrand *et al.* [25] has to be extended to cavities without mirror-reflection symmetry. This nontrivial extension to a degenerate perturbation theory is the topic of future work.

ACKNOWLEDGMENT

Financial support by the DFG (Project No. WI1986/7-1) is acknowledged. We also thank J. Kullig for discussions.

[1] K. J. Vahala, Nature (London) **424**, 839 (2003).
[2] S. L. McCall, A. F. J. Levi, R. E. Slusher, S. J. Pearton, and R. A. Logan, Appl. Phys. Lett. **60**, 289 (1992).
[3] C. P. Michael, K. Srinivasan, T. J. Johnson, O. Painter, K. H. Lee, K. Hennessy, H. Kim, and E. Hu, Appl. Phys. Lett. **90**, 051108 (2007).
[4] M. Witzany, R. Roßbach, W.-M. Schulz, M. Jetter, P. Michler, T.-L. Liu, E. Hu, J. Wiersig, and F. Jahnke, Phys. Rev. B **83**, 205305 (2011).
[5] A. F. J. Levi, R. E. Slusher, S. L. McCall, J. L. Glass, S. J. Pearton, and R. A. Logan, Appl. Phys. Lett. **62**, 561 (1993).
[6] J. U. Nöckel and A. D. Stone, Nature (London) **385**, 45 (1997).
[7] C. Gmachl, F. Capasso, E. E. Narimanov, J. U. Nöckel, A. D. Stone, J. Faist, D. L. Sivco, and A. Y. Cho, Science **280**, 1556 (1998).
[8] S. B. Lee, J. H. Lee, J. S. Chang, H. J. Moon, S. W. Kim, and K. An, Phys. Rev. Lett. **88**, 033903 (2002).
[9] H. G. L. Schwefel, N. B. Rex, H. E. Tureci, R. K. Chang, A. D. Stone, T. Ben-Messaoud, and J. Zyss, J. Opt. Soc. Am. B **21**, 923 (2004).
[10] G. D. Chern, H. E. Tureci, A. D. Stone, R. K. Chang, M. Kneissl, and N. M. Johnson, Appl. Phys. Lett. **83**, 1710 (2003).
[11] J. Wiersig and M. Hentschel, Phys. Rev. Lett. **100**, 033901 (2008).
[12] M. Hentschel and T.-Y. Kwon, Opt. Lett. **34**, 163 (2009).
[13] M. Hentschel, T.-Y. Kwon, M. A. Belkin, R. Audet, and F. Capasso, Opt. Express **17**, 10335 (2009).
[14] Q. H. Song, W. Fang, B. Liu, S. T. Ho, G. S. Solomon, and H. Cao, Phys. Rev. A **80**, 041807(R) (2009).
[15] C. Yan, Q. J. Wang, L. Diehl, M. Hentschel, J. Wiersig, N. Yu, Pfügel, F. Capasso, M. A. Belkin, T. Edamura *et al.*, Appl. Phys. Lett. **94**, 251101 (2009).
[16] S. Shinohara, M. Hentschel, J. Wiersig, T. Sasaki, and T. Harayama, Phys. Rev. A **80**, 031801(R) (2009).
[17] C.-H. Yi, M.-W. Kim, and C.-M. Kim, Appl. Phys. Lett. **95**, 141107 (2009).
[18] Q. H. Song, L. Ge, A. D. Stone, H. Cao, J. Wiersig, J.-B. Shim, J. Unterhinninghofen, W. Fang, and G. S. Solomon, Phys. Rev. Lett. **105**, 103902 (2010).
[19] F. Albert, C. Hopfmann, A. Eberspächer, F. Arnold, M. Emmerling, C. Schneider, S. Höfling, A. Forchel, M. Kamp, J. Wiersig *et al.*, Appl. Phys. Lett **101**, 021116 (2012).
[20] S. V. Boriskina, T. M. Benson, P. Sewell, and A. Nosich, IEEE J. Sel. Top. Quantum Electron. **12**, 52 (2006).
[21] Q. J. Wang, C. Yan, N. Yu, J. Unterhinninghofen, J. Wiersig, C. Pflügl, L. Diehl, T. Edamura, M. Yamanishi, H. Kan *et al.*, Proc. Natl. Acad. Sci. USA **107**, 22407 (2010).
[22] X.-F. Jiang, Y.-F. Xiao, C.-L. Zou, L. He, C.-H. Dong, B.-B. Li, Y. Li, F.-W. Sun, L. Yang, and Q. Gong, Adv. Mater. **24**, 260 (2012).
[23] M. Schermer, S. Bittner, G. Singh, C. Ulysee, M. Lebental, and J. Wiersig, Appl. Phys. Lett. **106**, 101107 (2015).
[24] H. Cao and J. Wiersig, Rev. Mod. Phys. **87**, 61 (2015).
[25] R. Dubertrand, E. Bogomolny, N. Djellali, M. Lebental, and C. Schmit, Phys. Rev. A **77**, 013804 (2008).
[26] L. Ge, Q. H. Song, B. Redding, and H. Cao, Phys. Rev. A **87**, 023833 (2013).
[27] J. Wiersig, Phys. Rev. A **85**, 063838 (2012).
[28] M. Kraft and J. Wiersig, Phys. Rev. A **89**, 023819 (2014).
[29] L. Ge, Q. Song, B. Redding, A. Eberspächer, J. Wiersig, and H. Cao, Phys. Rev. A **88**, 043801 (2013).
[30] Z. Ballard, M. Baaske, and F. Vollmer, Sensors **15**, 8968 (2015).
[31] A. Tarantola, *Inverse Problem Theory* (SIAM, Philadelphia, 2005).
[32] T. Hisch, M. Liertzer, D. Pogany, F. Mintert, and S. Rotter, Phys. Rev. Lett. **111**, 023902 (2013).
[33] S. F. Liew, B. Redding, L. Ge, G. S. Solomon, and H. Cao, Appl. Phys. Lett. **104**, 231108 (2014).
[34] D. R. Rhodes, IEEE Trans. Antennas Propag. **11**, 440 (1963).
[35] B. D. Sleeman, IMA J. Appl. Math. **29**, 113 (1982).
[36] M. Kac, Am. Math. Mon. **73**, 1 (1966).
[37] C. Gordon, D. Webb, and S. Wolpert, Inv. Math. **110**, 1 (1992).
[38] R. Sarma, L. Ge, J. Wiersig, and H. Cao, Phys. Rev. Lett. **114**, 053903 (2015).
[39] J. Kullig and Wiersig, New J. Phys. **18**, 015005 (2016).

[40] J. Wiersig, J. Opt. A **5**, 53 (2003).
[41] Q. Li, A. A. Eftehkar, Z. Xia, and A. Adibi, Opt. Lett. **37**, 1586 (2012).
[42] S. Lacey, H. Wang, D. H. Foster, and J. U. Nöckel, Phys. Rev. Lett. **91**, 033902 (2003).
[43] S. C. Creagh, Phys. Rev. Lett. **98**, 153901 (2007).
[44] S. C. Creagh and M. M. White, Phys. Rev. E **85**, 015201(R) (2012).
[45] J. Unterhinninghofen, Ph.D. thesis, Otto-von-Guericke-Universität Magdeburg (2011).